Chemistry
A European
Journal

Chemistry Europe
European Chemical Societies Publishing

Accepted Article

Title: Unveiling the occurrence of Co(III) in NiCo layered electroactive hydroxides. The role of distorted environments

Authors: Víctor Oestreicher, Diego Hunt, Martín Mizrahi, Félix G Requejo, and Matías Jobbágy

To be cited as: *Chem. Eur. J.* 10.1002/chem.202001944

Link to VoR: https://doi.org/10.1002/chem.202001944

WILEY-VCH

10.1002/chem.202001944

Unveiling the occurrence of Co(III) in NiCo layered electroactive hydroxides: the role of distorted environments

Diego Hunt,*[1#] Víctor Oestreicher,*[2#≠] Martin Mizrahi,[3,4] Felix G. Requejo,[3] and Matías Jobbágy*[2]

[1] *Departamento de Física de la Materia Condensada, GIyA, CAC-CNEA. Instituto de Nanociencia y Nanotecnología, CNEA-CONICET, San Martin, Buenos Aires B1650, Argentina.*

[2] *INQUIMAE-DQIAQF, Facultad de Ciencias Exactas y Naturales, Universidad de Buenos Aires. Ciudad Universitaria, Pab. II, C1428EHA, Buenos Aires, Argentina.*

[3] *Instituto de Investigaciones Fisicoquímicas Teóricas y Aplicadas (INIFTA), Departamento de Química, Facultad de Ciencias Exactas, Universidad Nacional de La Plata. CCT La Plata- CONICET, Diagonal 113 y 64, 1900, La Plata, Argentina.*

[4] *Facultad de Ingeniería, Universidad Nacional de La Plata, calle 1 esq. 47, 1900, La Plata, Argentina.*

Corresponding authors: hunt@tandar.cnea.gov.ar - victor.oestreicher@uv.es - jobbag@qi.fcen.uba.ar

[≠]Current address: *Instituto de Ciencia Molecular (ICMol), Universidad de Valencia, Catedrático José Betrán 2, 46980 Valencia, Spain*

[#]These authors contributed equally to this work.

10.1002/chem.202001944

Co- and Ni-based layered hydroxides constitute a unique class of two-dimensional inorganic materials with exceptional chemical diversity, physicochemical properties and outstanding performance as supercapacitors and overall water splitting catalysts. Recently, the occurrence of Co(III) in these phases has been proposed as a key factor that enhance their electrochemical performance. However, the origin of this centers and control over its contents remains as an open question. We employed the Epoxide Route to synthesize a whole set of α-NiCo layered hydroxides. The PXRD and XAS characterization alert about the occurrence of Co(III) as a consequence of the increment in the Ni content. DFT+U simulation suggest that the shortening of the Co–O distance promotes a structural distortion in the Co environments, resulting in a double degeneration in the octahedral Co 3d orbitals. Hence, a strong modification of the electronic properties leaves the system prone to oxidation, by the appearance of Co localized electronic states on the Fermi level. This work combines a microscopic interpretation supported by a multiscale crystallochemical analysis, regarding the so called synergistic redox behavior of Co and Ni, offering fundamental tools for the controllable design of highly efficient electroactive materials. To the best of our knowledge this is the first computational-experimental investigation of the electronic and structural details of α-NiCo hydroxides, laying the foundation for the fine tuning of electronic properties in layered hydroxides.

Introduction

The global demand for sustainable energy triggered a massive effort to develop efficient, low-cost alternative materials and devices for clean energy generation and storage.[1,2] Electrochemical-based platforms as water splitting cells and supercapacitive devices have demonstrated to be able to play both roles.[3,4,5] Nowadays, two-dimensional (2D) materials, such graphene and other layered materials, arise as exceptional candidates to improve the current status in this field.[6, 7,8] Among the most promising members of the 2D materials family, those based on earth abundant[9] and non-geolocalized transition metals, such as layered multicationic oxides,[10] hydroxides,[11] sulfides,[12] among others,[13] play a leading role in the race for efficient aqueous based supercapacitors and water splitting devices. One particular family of compounds, the NiCo hydroxides, were recently studied for both applications by numerous authors, revealing their outstanding electrochemical performances.[14,15,16,17] The combination of both metal ions results in a synergic effect optimizing both capacitance and electrical conductivity.[18,19] However, most of the current efforts in optimizing these materials rely on a trial and error screening, either based on crystallochemical or textural modifications.[20,21] The former includes modifications of the crystal structure, Ni to Co ratio,[22] and interlayer anions in order to modulate interlayer distances (diffusion) and hydrophobicity (inorganic *vs.* organic anions), respectively;[23] screening of textural modifications includes tuning particle sizes and shapes and, eventually, the exfoliation into single layers.[24] Finally, in order to increase the conductivity, a proper dispersion of these phases within a conductive substrate, or direct growth on an electrode (such as Ni foam or carbon-based supports) has to be realized.[25,26] Therefore, it is not surprising that in such multivariate experimental scenarios, the optimum formulation is crucially depending on the preparational methods and remains matter of debate, taking the inherent complexity of these electrochemical assemblies into account. Meanwhile, fundamental aspects related to the electronic and crystallochemical nature of these compounds remain poorly understood. These hydroxides are indistinctly defined as α-hydroxides and/or LDHs phases just for the mere fact of being expanded along their interbasal axis (*c* parameter), compared to the β-hydroxides, also known as *Brucite*-like layered phases.[15] This inherently imprecise description ignores key aspects as the stacking order-disorder of the layers (*xy* planes), the presence of defects, the occurrence of oxidized cations and/or non-octahedral coordination environments and the inherent nature of anion-layer interactions (covalent

vs electrostatic), among others. Moreover, *in silico* simulations of simplified and unrealistic structures tend to offer a risky scenario for the prediction of electronic structure. For example, for NiCo layered hydroxides synthesized by homogenous methods, the occurrence of Co(III) in the presence of oxygen was reported, while at the same time the bare Co endmember remained unaltered.[20,24,27,28] It is important to point out, that the Co(III):Co(II) ratio can have an effect on the active sites in the redox reaction, while the increment of this ratio leads to a significant enhancement of the specific capacitance.[29] Moreover, Density Functional Theory (DFT) calculations suggest, that the presence of certain trivalent cations can affect the electrochemical behavior through a band gap modification.[30] Hence, the occurrence of Co(III) in these materials must be understood in order to thoroughly rationalize the design and physical properties of these compounds.

In parallel to experimental approaches, DFT based studies are widely employed to complement the exploration of materials for energy conversion and storage.[31] Ranging from studies of ion intercalation structures to elucidate the underlying mechanisms of energy storage,[32] to the evaluation of the performance of oxygen reduction reaction (ORR), oxygen evolution reaction (OER), and hydrogen evolution reaction (HER),[33] the theoretical calculations based on DFT represent powerful and promising techniques to complement studies in the energy field. However, 2D-materials based on transition metal ions require a proper description, accounting for their inherently high electronic correlation contribution of their respective *d* shell electrons. The incorporation of the Hubbard term in the Kohn-Sham Hamiltonian (DFT+U)[34] has been accepted as an accurate tool for describing the electronic structure of transition metal layered hydroxides,[35,36] offering less expensive calculations than those based on hybrid functionals. While many reports based on DFT+U are focused on the electrochemical properties of water oxidation on *e.g.* 2D NiCo layered hydroxides and related compounds, [30,37,38,39,40,41,] there are very few reports focused on the fundamental comprehension of structural properties and electronic structure of theses phases. A microscopic understanding of the electronic structures and structural environments of Ni and Co ions inside the layers are necessary for a reliable in-depth study of their physical and physicochemical properties. In addition, in order to correlate the DFT+U calculation with the experimental data, the intrinsic behavior of each constituent (oxidation state, average coordination number, interatomic distances and degree of disorder for each atom) must

be assessed by an element-selective technique, such as X-ray Absorption Spectroscopy (XAS), with local atomic-order sensitivity.[42,43,44]

In search of the chemical aspects that control the occurrence of Co(III) in NiCo layered hydroxides, we envisaged a systematic exploration of nanotextured α-NiCo hydroxides,[45] obtained through the *Epoxide Route*.[46] This one pot room temperature method drives the precipitation under extremely mild conditions, offering a reliable tool to crystallize nano layered hydroxides containing diverse cations[47] and/or interlamellar anions[48] The specimens were thoroughly characterized by PXRD, UV-Vis, SEM, and XANES-EXAFS, showing the dependence of Co(III) on the respective Ni content. Meanwhile, a microscopic description, provided by DFT+U depicts an extraordinary change on the electronic properties of the system, modulated by the incorporation of Ni atoms into the α-Co hydroxide supercell. These new states above the Fermi level are associated with octahedral Co atoms, exclusively, and they are a consequence of the octahedral environment distortion. A detailed inspection of those Co(II) ions exclude a double degeneration on the *3d* orbitals, allowing their potential oxidation to Co(III). To the best of our knowledge, this is the first report of a "*cis distortion*" in layered hydroxides, paving the way to the rational design of 2D hydroxides for energy storage and conversion.

Results and Discussion

A set of NiCo layered hydroxides were synthesized through the *Epoxide Route* in a one pot reaction according to our previous report.[45] This homogeneous alkalinization reaction, in contrast to those, based on ammonium releasing reagent (ARR), takes place at room temperature allowing the precipitation of layered hydroxide without phase segregation[49] or the contamination with carbonates. This allows the crystallization of novel layered hydroxide compounds with tunable electrical properties.[50] In addition, the final pH in this method is not constrained by the presence of the ammonia/ammonium buffer, therefore allows final pH values higher than 10 to be easily achieved, ensuring the quantitative precipitation of most transition metal cations. Samples are labeled as NiX (with $0 \leq X \leq 100$), where X accounts for the total Ni percentage in the sample. The PXRD patterns recorded for all samples are compiled in Figure 1A, confirming the layered nature of the whole family, and evidenced by characteristic interlamellar signals in the *2-theta* range between 5º and 20º. However, differences arise with increasing Ni content. Starting from sample Ni0, the pure cobalt-based sample presents all the main diffraction signals

reported for the α-Co(II) hydroxide, a layered basic chloride described by the general formula, $Co(OH)_{2-x}Cl_x \cdot mH_2O$ (see Figure S1).[51] This phase is defined by predominant occupation of octahedral Co(II) centers, hereafter denoted as Co(II)^{Oh}, which display a bidimensional infinite hexagonal arrangement of cations, chemically bound trough μ3-OH bridges, as in the parent perfectly regular lattice of β-$Co(OH)_2$, also known as brucitic phase.[35] Nevertheless, Co(II) ions can adopt diverse coordination environments;[52] in the particular case of the α-Co(II) hydroxide phase, certain Co(II)^{Oh} positions of each layer can remain vacant, and these sites will be occupied by a pair of tetrahedral centered Co(II)^{Td}, placed outside the brucitic hydroxylated layer (see Scheme 1). Each of the Co(II)^{Td} is then coordinated to three OH groups belonging to the brucitic layer, meanwhile the fourth coordination position is occupied by chloride anions, as found in the well-defined structure of mineral *Simonkolleite*, $Zn_3^{Oh}Zn_2^{Td}(OH)_8Cl_2 \cdot mH_2O$.[53] However, the crystalline Co(II) phase follows a less defined formula, $Co_{1-x}^{Oh}Co_x^{Td}(OH)_{2-x}Cl_x \cdot mH_2O$,[54] holding a predominant fraction of octahedral centers, with an $0.05 \leq x \leq 0.40$ value that depends on the preparation method and the interlayer halide[50] and is characterized by a disordered-clustered distribution of Co(II)^{Td} sites within the layers.[55,56]

On the other hand, sample Ni100 depicts all signals reported for the α-Ni(II) hydroxide phase in which the layered structure is governed by a turbostratic disorder, defined by a relative rotation of successively stacked layers.[57] This structure, obeys the formula $Ni(OH)_{2-x}A_{x/n} \cdot mH_2O$, where A^{n-} represents an exchangeable anion, with Ni(II) centers located in octahedral environment, Ni(II)^{Oh}, exclusively.[58] Beside this, α-Ni(II) hydroxide phases resemble the structure of LDH compounds; it is important to point out non-trivalent cations are present within the layers, while the structural nature of this kind of layered hydroxide material still remains to be an open question.[59,60]

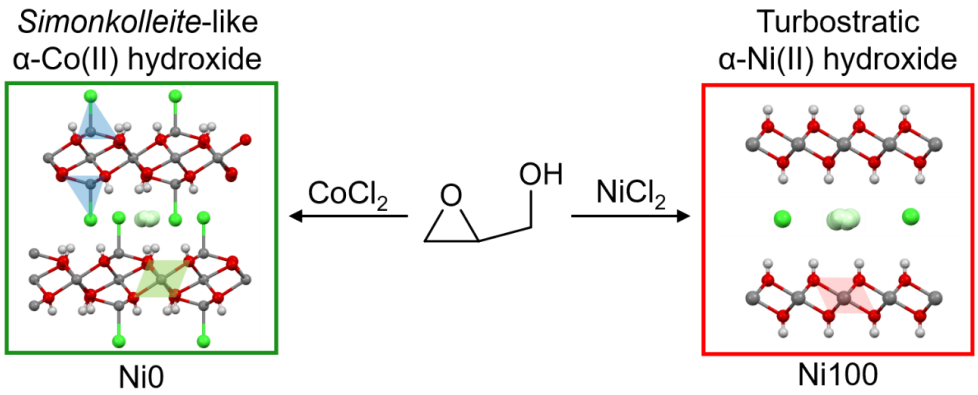

Scheme 1. α-layered hydroxides obtained through the Epoxide Route (46) employing $CoCl_2$ (left) or $NiCl_2$ (right) precursors. Ni0 results in a *Simonkolleite*-like structure, where Co(II) ions occupy two crystallographic environments: octahedral (green) and tetrahedral (blue). Ni100 results in a highly defective *Brucite*-like (turbostratic) structure, where all the Ni(II) ions are located within an octahedral environment (red).

Concerning the intermediate binary samples, once part of the Co ions are increasingly replaced by Ni ones form the initial solution, all the main diffraction signals observed along the 30º < *2-theta* < 40º and 50º < *2-theta* < 62º ranges depict a monotonous shift towards higher angles, or shorter interatomic distances, in perfect agreement with the incorporation of a smaller cation (see Figure 1B). Interestingly, the basal plane spacing given by the *{003}* and *{006}* signals remains almost invariant for samples Ni0 to Ni75. However, up to the sample Ni80, highly coalesced diffraction signals are noticeable indicating an almost total turbostratic disorder. In addition, textural changes are evident by broadened diffraction peaks, occurring in the intra as well as interlamellar domains, indicating a hindered crystal growth due to the presence of Ni, as also corroborated by electron microscopy inspection (see Figure S2).

In order to provide further information regarding the environment of each cation, UV-Vis diffuse reflectance spectroscopy was performed (see Figure 1C). In the case of sample Ni0, the band present in the range of 400 - 550 nm results from a contribution of two peaks commonly centered at 470 and 530 nm, belonging to the of $^4T_{1g}$ to $^4T_{1g}$(P) and $^4A_{2g}$(F) transitions of Co(II)^{Oh} coordinated by weak-field ligands. In addition, an inherently intense band around 600 – 700 nm can be assigned to the $^4A_2$(F) to $^4T_1$(P) transition of Co(II)^{Td}.[51,61] In the opposite extreme, the sample Ni100 presents three bands centered at 400, 680 and 760 nm belonging to $^3A_{2g}$ to $^3T_{1g}$(P), $^3T_{1g}$(F), and ^1E_g(D) transitions of Ni(II)^{Oh}, respectively.[62] Most binary samples can be interpreted on the basis of a decreasing contribution of the Co(II)^{Oh} and Co(II)^{Td} bands accompanied by a rise of

the signal ascribed to the Ni(II)^{Oh} characteristic bands. Nevertheless, sample Ni90 does not follow this trend since the characteristic sharp bands centered around 600 – 700 nm are practically missing, suggesting the absence of Co(II)^{Td}. Figure 1D presents the dependence of basal space (calculated as $d_{BS} = ½ [d_{003} + 2 \cdot d_{006}]$), deduced from *{003}* and *{006}* reflections as well as the intralayer average cation-to-cation distance (*a* parameter), proportional to the *{110}* reflection (calculated as $d_{intra} = 2 \cdot d_{110}$).

Besides the structural parameters on both ends of the specimen family, Ni0 and Ni100, coincide with the chloride containing α-hydroxides reported before.[51,63] Two scenarios are noticeable for the binary phases. While samples from Ni0 to Ni80 adopt the *Simonkolleite*-like structure with Co(II)^{Td} (blue zone), where the cation-to-cation average distance contracts with increasing Ni(II) contents, the tendency and magnitude of this distortion is similar to the one observed for hydrothermally-aged brucitic $\beta - Co_{1-x}Ni_x\ (OH)_2$ solid solutions obtained by ARR methods;[64] and obeys to the inherent differences in ionic radii ($R_{Co(II)^{oh}} = 0.745$ Å; $R_{Ni(II)^{oh}} = 0.69$ Å).[65]

Nowadays there is a generalized misunderstanding in the literature concerning the structure of these phases, frequently considered as LDHs.[15] Therefore, at this point it is important to highlight that, unlike to the LDHs structure in which M(II) and M(III) coexist with the same coordination environment, in the α-NiCo layered hydroxides, both ions have divalent oxidation state, *i.e.* Co(II) and Ni(II), independently of the coordination environment excluding the existence of M(III). Moreover, while in the case of LDHs the interaction between the interlayer anion and the solid is purely electrostatic, in the case of Co-rich α-layered hydroxides the anion is covalently linked to specific sites belonging to the layers.

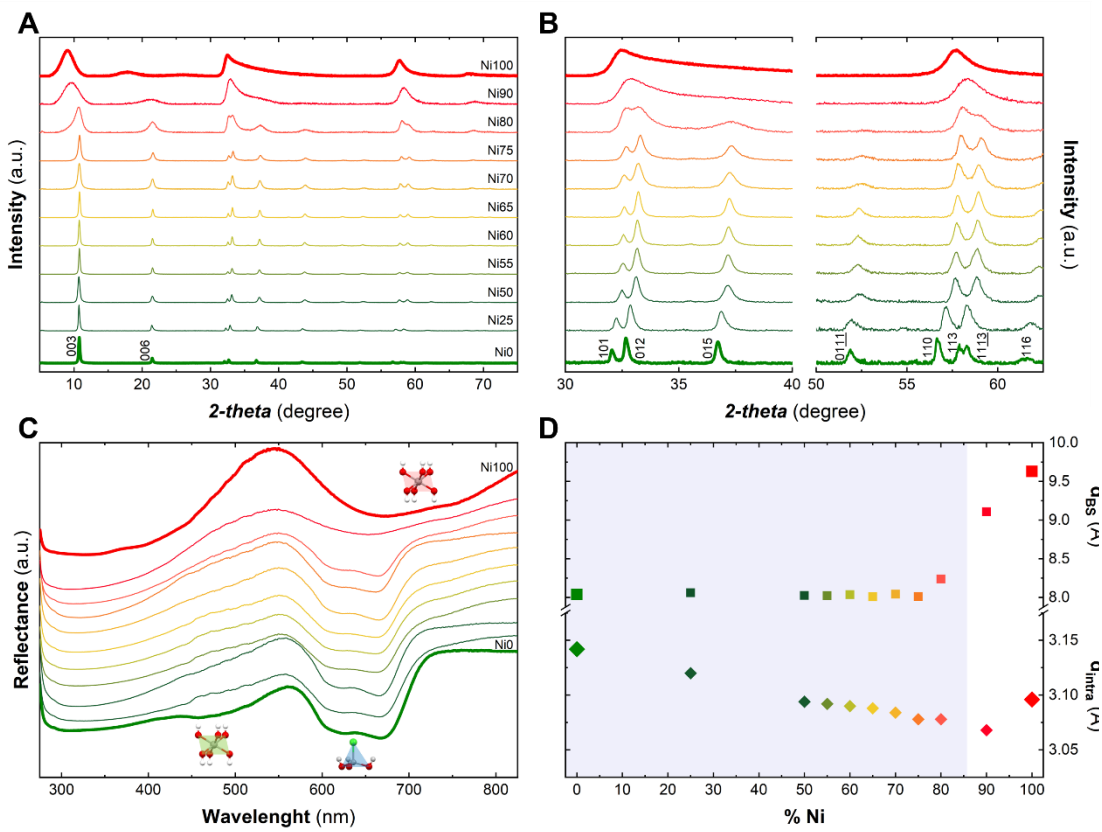

Figure 1. (A) PXRD patterns recorded along the 5 – 75º range for the whole set of NiCo samples. synthesized. (B) Zoom-in PXRD patterns between 30 – 40º and 50 – 62º. Sample Ni0 or α-Co(II) hydroxide were indexed according to reference.[52] (C) UV-Vis spectra (diffuse reflectance mode) as a function of the chemical composition. The absorption bands are attributed to the transition energy corresponding to Co(II) in tetrahedral (650 nm) and octahedral (500 nm) environments, as well as Ni(II) in octahedral environment (675 nm and 750 nm). (D) Characteristic *a* and *c* cell parameters, expressed as d_{intra} (intralayer cation to cation distance) and d_{BS} (interlayer cation-to-cation distance), as a function of the Ni(II) content. The blue zone depicts the compositional range in which Co(II)^{Td} is present within the structure. All the samples were synthesized at room temperature employing: [$CoCl_2$+$NiCl_2$] = 10 mM, [NaCl] = 100 mM, [Gly] = 400 mM, ageing for 48 h.

In order to provide element-specific structural and chemical insights, all samples were characterized by X-Ray Absorption Spectroscopy (XAS) – near edge (XANES) as well as extended edge (EXAFS) –. Figure 2 depicts the Co and Ni K-edges XANES fingerprints. For the Ni K-edge spectra (Figure 2-left) no variation in the position of the absorption edge (vertical black line) as a function of Ni content is observable, being comparable to the pure reference β-$Ni(OH)_2$. These results confirm that Ni(II) ions are immersed in an octahedral environment exclusively, as previously observed for related phases (Figure S3).[66,67] Nevertheless, in the case of Co K-edge spectra a net shift in the absorption edge position towards higher energy values can be noticed for Ni(II) contents

10.1002/chem.202001944

higher than 60% (Figure 2-right). This shift can be associated with an increment in the average oxidation state of the Co atoms, which practically reaches the value for Co(III) reference in the sample Ni90 (see Figure S4). These results provide the first indication regarding the modulation of Co(III) fraction as a function of the Ni(II) content (see Figure S5). Interestingly, samples with increasing concentration of Co(III) present higher values of specific capacitance, as reported by us before.[45]

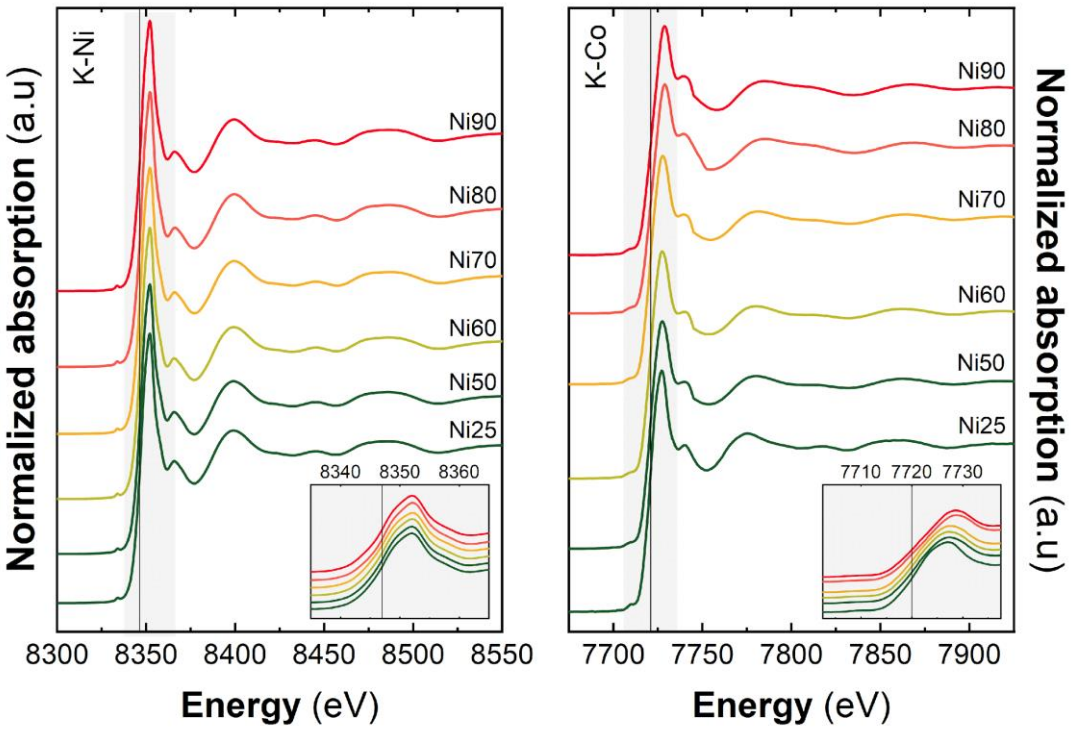

Figure 2. Normalized XANES spectra of Ni K-edge (left) and Co K-edge (right) recorded for samples Ni25 to Ni90. Insets: Detail of the absorption edge region.

Figure 3A-left shows the oscillations of the extended regions of the absorption spectra (EXAFS) at the Ni K-edges. The oscillations, as well as their corresponding Fourier Transformations (FT) (Figure 3B-left), which can be interpreted as a *pseudo*-distribution of the interatomic distances to the absorbing atoms, are comparable. These results confirm that the Ni atomic environment remains practically unaltered for all samples. However, in the case of Co K-edge, the samples experience a noticeable change with the Ni increment. A new contribution starts to arise from sample Ni60, being consolidated from sample Ni80 (gray zone, Figure 3A-right) and indicating that Co atoms tend to be in a much more defined coordination environment in terms of interatomic distances and number of nearest neighbors.

10.1002/chem.202001944

In the case of the FT for the EXAFS oscillations at the Co K-edge (Figure 3B-right), there are two major contributions along the 1 – 3 $Å^{-1}$ range, that represent the average distances to the first and second coordination shell around the Co atoms, respectively. Regarding the first peak, the full width at half maximum (FWHM) is higher for samples with low Ni contents, suggesting this signal combines two Co–O distances of similar magnitude – $Co(II)^{Oh}$ and $Co(II)^{Td}$ –. Analogously, the smaller amplitude of this first peak in the low Ni content, may be associated with the presence of more than one coordination sphere, confirming the coexistence of $Co(II)^{Oh}$ and $Co(II)^{Td}$. This is furthermore in good agreement with our UV-Vis characterization (see Figure 1-C).

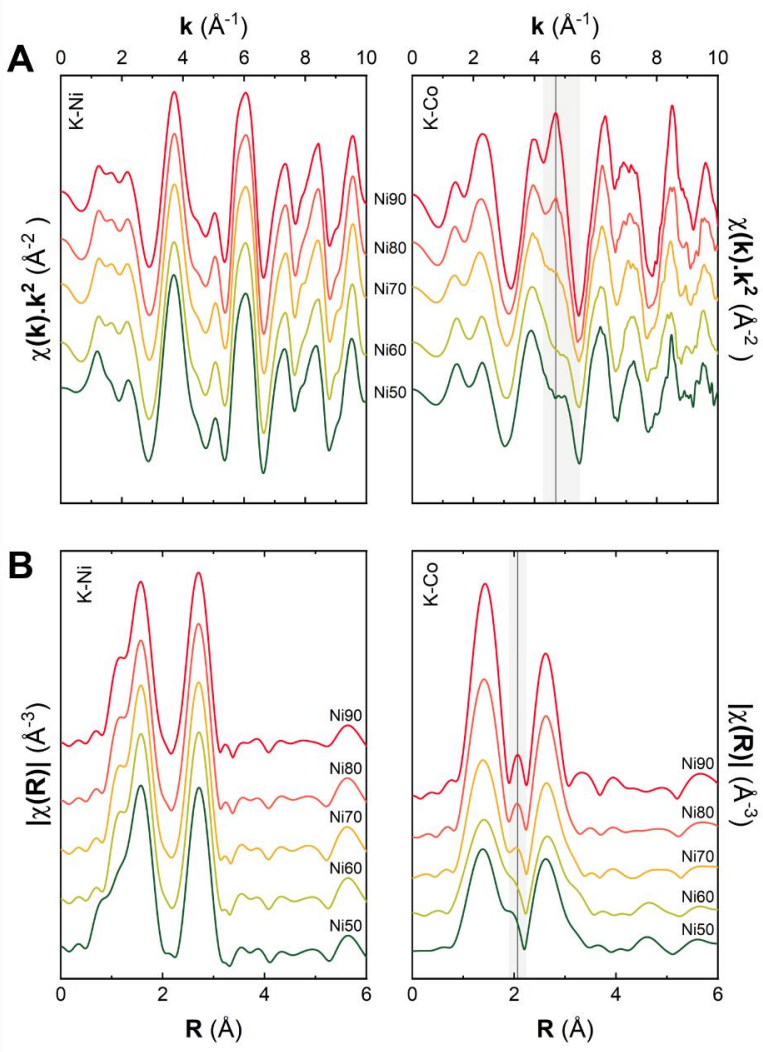

Figure 3. (A) EXAFS oscillations for Ni K-edge (left) and Co K-edge (right), and (B) their corresponding Fourier transforms for the samples Ni50 to Ni90.

EXAFS fits were performed in order to obtain the structural parameters as average coordination numbers (N), interatomic distances (R) and structural disorder parameter

(σ^2) for each cation. Figure S6 depicts the fits at the Ni K-edge where a two coordination shell model was proposed, one for the first oxygen neighbors (Ni–O) and another for the second neighbors (Ni–Ni,Co atoms). The results obtained from the fits (see Table S1) show, that the first coordination sphere hosts 6 oxygen atoms at an average distance R_{Ni-O} of 2.04 Å, while the second sphere holds 6 Ni or Co atoms at an average distance $R_{Ni-Ni,Co}$ of 3.08 Å, for all samples. Each of these values are in excellent agreement with those expected for a Ni(II) occupancy in octahedral sites,[68] confirming the structural invariance along the composition.

However, due to the more complex signals recorded at Co-K edge, different models were employed according to the composition (see Figure S7). In samples up to a Ni content of 70%, two Co–O coordination spheres, describing Co^{Td} and Co^{Oh} sites were employed (in concordance with UV-Vis measurements). We completed the atomic environment by accounting for a third coordination sphere of Co,Ni atoms taking into account Co–Co,Ni distances in both environments. The obtained Co–O distances of 1.89 Å and 2.14 Å, are in excellent agreement with the crystallographic data reported for α-Co(II) hydroxide.[52] In the other set (above 70% of Ni content), Co–O environments of sample Ni80 and Ni90 were properly described by Co^{Oh} sites exclusively (see Table S2). The shortening of Co–O distance of 2.10 Å results from an increasing oxidation of Co ions towards the trivalent state ($R_{Co(II)^{Oh}} = 0.745$ Å; $R_{Co(III)^{Oh}} = 0.61$ Å).[65,69] After the understanding of the structural impact of increasing Co(III) contents as a function of Ni(II) substitution, a microscopic description by DFT+U was required to envision the chemical basis for this tendency for oxidation.

In the context of based DFT+U calculations, we have optimized the Hubbard parameter (U) for Co atoms in the case of β-$Co(OH)_2$, reproducing correctly the magnetic properties of this phase.[35] Then we realize a systematic computational study of the structural and magnetic properties of a layered family of α-Co(II) hydroxichlorides, analyzing the influence of U on the electronic and magnetic behavior.[36] Finally, we demonstrated an excellent correlation between the experimental measurements and theoretical results, concerning to electrical and magnetic properties of α-Co(II) hydroxyhalide family compounds.[50]

As a first step to provide an atomistic description of the electronic structure of these 2D α-NiCo layered hydroxides, it is mandatory to establish the most stable configurations in terms of occupation of tetrahedral positions. To investigate the crystallographic

distribution, a *Simonkolleite*-like family of representative lattices, obeying the general formula $(Co, Ni)_8^{Oh}(Co, Ni)_2^{Td}(OH)_{18}Cl_2$ was analyzed by means of DFT+U calculations. For any Ni:Co ratio, the extreme scenario, in which all the tetrahedral sites were occupied exclusively by Co(II), following the formula $Ni_{8-n}^{Oh}Co_n^{Oh}Co_2^{Td}(OH)_{18}Cl_2$, remained more stable than the counterparts where all the tetrahedral sites were occupied by Ni(II) ions, following the formula $Ni_{6-n}^{Oh}Co_{n+2}^{Oh}Ni_2^{Td}(OH)_{18}Cl_2$ (see Figure S8 and S9). In all cases, the energy differences were calculated taking into account an antiferromagnetic coupling between the two types of ions environment, as we have previously reported.[36,50] Hence, DFT+U calculations confirm the occurrence of a specific occupation of tetrahedral sites by Co(II) ions in perfect agreement with UV-Vis and EXAFS characterization.

After establishing the stable configuration of these phases, ruled by the presence of Co(II)^{Td} exclusively, supercells with the formula $Ni_{15-n}^{Oh}Co_n^{Oh}Co_2^{Td}(OH)_{32}Cl_2$ (with $3 \leq n \leq 14$) were simulated in order to study the influence of Ni^{Oh}:Co^{Oh} ratio over the electronic structure of these lattices. For this set of structures, the environment of Co^{Td}, defined by the Co^{Td}–OH and Co^{Td}–Cl distances remains invariant even for the supercell containing Co(II)^{Td} exclusively ($Ni_{15}^{Oh}Co_2^{Td}(OH)_{32}Cl_2$), confirming the inherent rigidity of these units observed by EXAFS. Figure 4 depicts the Projected Density of States (PDOS) belonging to four different supercells: $Ni_{DFT+U}29$ ($Ni_5^{Oh}Co_{10}^{Oh}Co_2^{Td}(OH)_{16}Cl_2$), $Ni_{DFT+U}58$ ($Ni_{10}^{Oh}Co_5^{Oh}Co_2^{Td}(OH)_{16}Cl_2$), $Ni_{DFT+U}65$ ($Ni_{11}^{Oh}Co_4^{Oh}Co_2^{Td}(OH)_{16}Cl_2$) and $Ni_{DFT+U}71$ ($Ni_{12}^{Oh}Co_3^{Oh}Co_2^{Td}(OH)_{16}Cl_2$), where 29, 58, 65 and 71 describe Ni content (as percentage of cationic positions) in the supercell. For low Ni contents, the electronic structure resembles that of the bare layered $Co^{Oh}{}_{15}Co^{Td}{}_2(OH)_{16}Cl_2$ where the *p* states of Cl and O atoms have a larger contribution to the valence bands with an E_{gap} ~ 1.6 eV. (Figure 4, panels A and B).[37] With the increment of Ni atoms in the supercell, the *d* orbitals from Ni(II) begin to add major contributions to the conduction bands (see Figure S10 and S11). However, the electronic structure drastically changes for samples $Ni_{DFT+U}65$ and $Ni_{DFT+U}71$ (Figure 4, panels C and D). Remarkably, in these cases, localized states belonging to certain specific Co^{Oh} centers appear on the Fermi level, turning the system prone to oxidation.

10.1002/chem.202001944

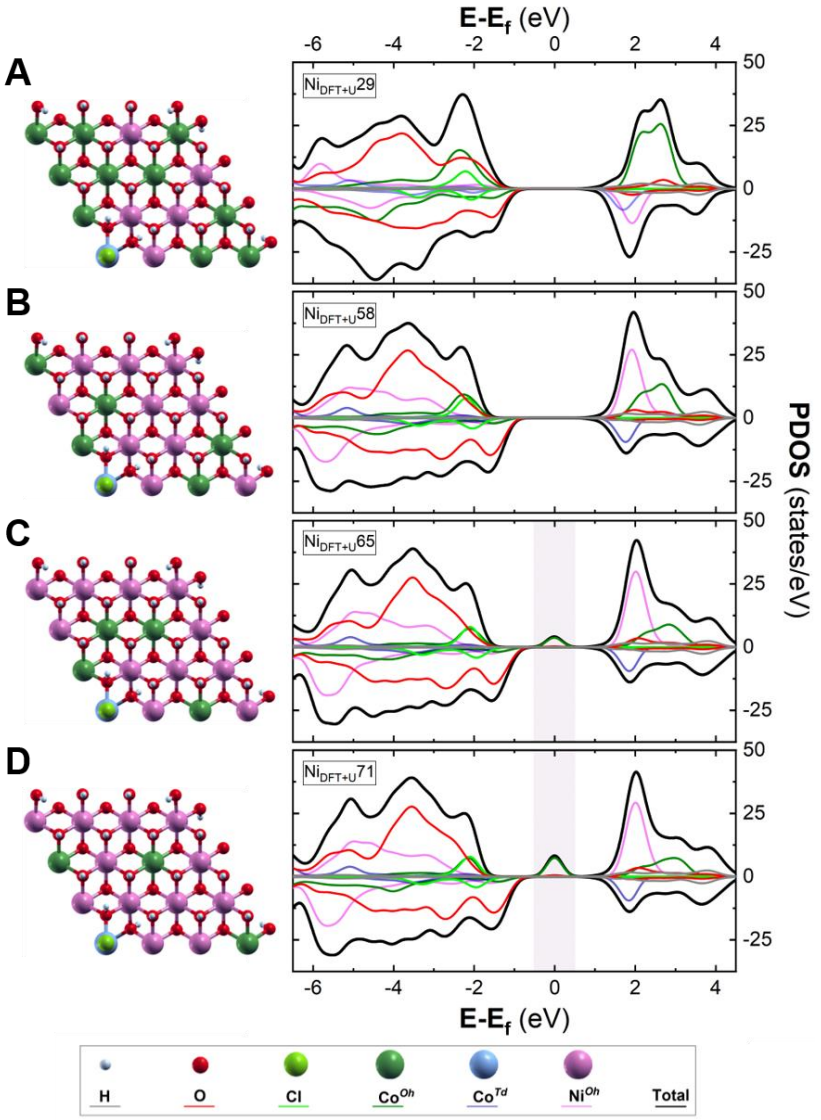

Figure 4. Total and projected density of states (PDOS) for a single layer of $Ni_{15-n}^{Oh}Co_n^{Oh}Co_2^{Td}(OH)_{32}Cl_2$ supercells with increasing Ni(II) contents. The Ni(II) content was denoted on the supercells with Ni_{DFT+U}(%Ni), being the %Ni 29(A), 58(B), 65(C) and 71(D). In gray is depicted the appearance of localized states form Co^{Oh} on the Fermi level.

In order to understand the dramatic changes on the electronic structure of *Simonkolleite*-like NiCo layered hydroxide, a detailed examination of the coordination environment of the Co^{Oh} atoms was carried out. Figure 5 depicts the electronic behavior of *d* orbitals for Co^{Oh} ions in $Ni_{DFT+U}29$ and $Ni_{DFT+U}65$ supercells. In the case of the lowest Ni content, their octahedral geometry remains identical to those of a pure α-Co(II) phase,[51] exhibiting Co^{Oh}–OH distances equal to 2.11 Å. Nevertheless, with the increment of Ni(II), the coordination sphere of Co^{Oh} ions experiences a structural distortion, that results in a compression-elongation of the Co–OH distances. The six Co^{Oh}–OH distances split into a

set of different values: four compressed distances of 2.10 Å and two elongated to 2.12 Å. This distorted environment promotes a double degeneration of the *d* orbitals, affecting mainly the d_{xy}, d_{zx}, d_{zy} and $d_{x^2-y^2}$ orbitals. Thus, new states on the Fermi level appear; the supercell $Ni_{DFT+U}71$ confirms the trend (see Figure S12). The local distortion of Co^{Oh} and lattice contraction suggested by the DFT+U calculations (see Figure S13) are in perfect agreement with the overall compression of the intralayer distances (or *a* parameters) obtained from PXRD (Figure 1D), as well as EXAFS analysis (see Table S1 and S2).

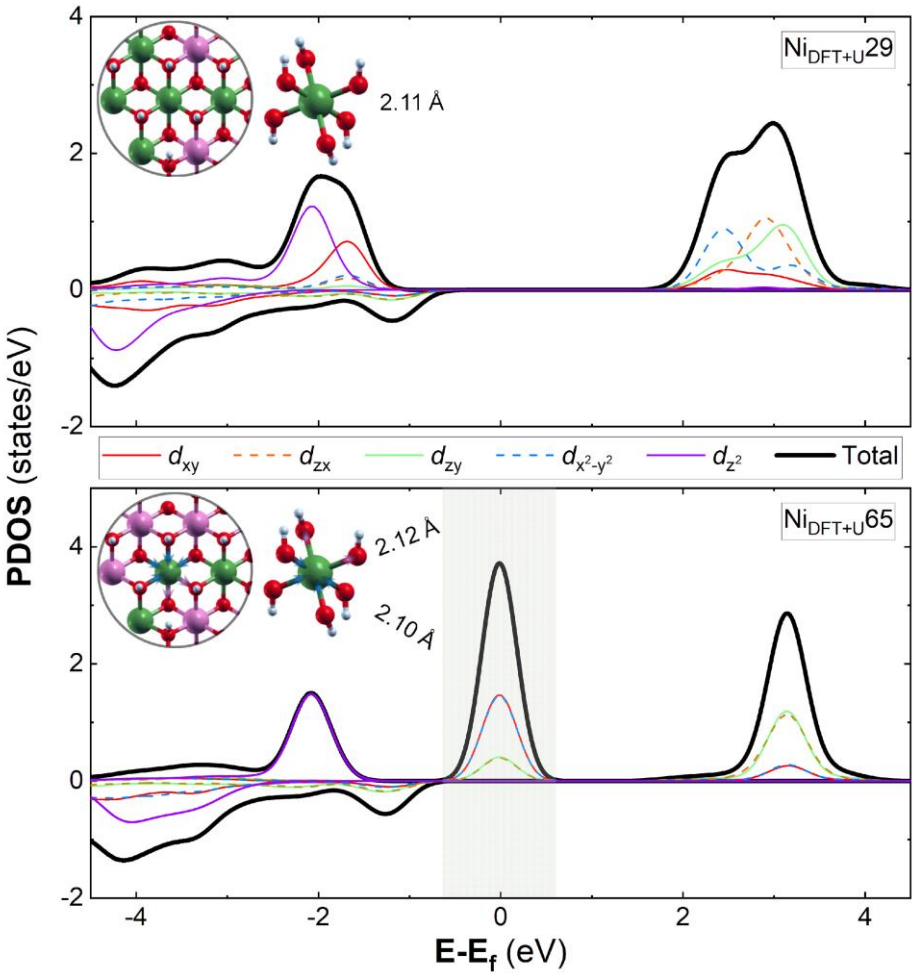

Figure 5. Projected density of states (PDOS) for the *d* orbitals corresponding to the two different Ni:Co ratio resulting in two Co(II) ions environments inside the layer. Upper panel depicts the $Ni_{DFT+U}29$ sample where Co(II) ions remain unaltered with respect to the bare Co structure. Lower panel depicts the $Ni_{DFT+U}65$ sample where the compression-elongation of the Co–OH distances promote the double degeneration of *d* orbitals known as "*cis distortion*". In gray is remarked the contribution of d_{xy}, d_{zx}, d_{zy} and $d_{x^2-y^2}$ orbitals in the localized states on the Fermi level.

This behavior known as "*cis distortion*",[70,71] has been reported before for six-fold-coordinated Cu(II) coordination compounds[72,73] as well as several clathrochelates metalloligands,[74,75] providing a versatile tool to tune the electronic properties of the metallic centers.[76] Moreover, this approach was recently employed to effectively stabilize highly oxidized centers as Fe(IV) in aqueous solution, under ambient conditions.[77] It is important to point out that these localized states are unstable and thermal fluctuations will promote the oxidation of Co centers. In our case, this kind of double degeneration resemble a high-spin d^7 metal ion with ideal tetragonal prism (D_{3h}) geometry, in which the magnetic anisotropy induced by first-order Spin Orbit Coupling (SOC) over the non-bonding *d* orbitals partially filled, induces the double degeneration of *d* orbitals[70,72,78,78,71] However, to the best of our knowledge this is the first report for layered hydroxides in which the so-called *"cis distortion"* can modify the electronic nature of 2D materials allowing the oxidation of the metallic centers and, hence, tune the electrochemical behavior of the resulting materials. Interestingly, the α-NiCo layered hydroxides analyzed in this work exhibit their optimum performance in terms of specific capacitance for compositions that hold significant fractions of Co(III), as we reported before.[45] Specifically, we found the higher specific capacitance of 2091 F/g (obtained at a discharge current density of 0.5 A/g) for samples with more than 80% of Ni.[45] Our previous electrochemical measurements, in agreement with over reports with hydroxylated phases containing Co(III),[20,24,27,28,29] support the current claims regarding the role of these oxidized centers in the improvement of electrochemical properties of α-NiCo layered hydroxides. In fact, the current experimental and computational findings, mutually confirm the occurrence of a new type of layered structure, where two different environments (octahedral and tetrahedral) and two oxidation states (divalent and trivalent) coexist. Then, this unique and inherently complex structure, herein named "meta layered hydroxide" (mLH), combines in a single phase the inherent functionalities of the layered double hydroxides and the simonkolleite-like layered basic salts.[87]

Conclusions

The description of the inherently complex structure of α-NiCo layered hydroxides, governed by the coexistence of Co^{Oh} and Co^{Td}, and Ni^{Oh} centres, can be simplified in terms of the interplay of inherently rigid units, Co^{Td}, and Ni^{Oh}, that share a common 2D lattice with more distortable Co^{Oh} centers. The proper synthetic tuning of the Ni:Co ratio results in a critical compressive force driven by Ni^{Oh} promoting a *"cis distortion"* over the Co^{Oh} units. These distorted Co^{Oh} centers tend to populate the Fermi level with their *d* states, enhancing their reactivity and allowing their oxidation to Co(III), resulting in increasing fractions of Co(III) centers stabilized in well-defined octahedral coordination environments that depend on the Ni(II) content. This finding clearly demonstrates how the stabilization of higher oxidation states is driven by a tuned coordination environment; a coordination chemistry concept that was traditionally restricted to molecular entities, can be naturally extended to synthetic 2D materials. The current study demonstrates on solid basis how an advanced synthetic method, as the *Epoxide Route*, allows to produce well-defined 2D compounds in which the tunable oxidation state of the transition metal cations can be designed and understood on rational basis, in order to enhance the electrochemical performance of these layered materials.

Acknowledgements

This work was supported by the University of Buenos Aires (UBACyT 20020130100610BA), the National University of La Plata (UNLP, project X654), the Agencia Nacional de Promoción Científica y Tecnológica (ANPCyT, projects: PICT 2012-1167, PICT 2015-2285 and PICT 2017-1220), the National Research Council of Argentina (CONICET PIP 11220110101020). VO and DH acknowledge CONICET for postdoctoral fellowship. MM, FR and MJ are Research Scientists of CONICET (Argentina). VO is member or ALN. The authors want to acknowledge Dr. Paula C. Angelomé for access to UV−Vis reflectance facilities and the inspiring moments. The authors thank Dr. Christian Dolle for the valuable discussion. Specially, we are deeply grateful to Prof. Damian Scherlis for his generous advice and fruitful comments.

Materials and Methods

Chemicals. Cobalt chloride hexahydrate ($CoCl_2.6H_2O$), nickel chloride hexahydrate ($NiCl_2.6H_2O$), sodium chloride (NaCl) and glycidol (Gly) were purchased form Sigma-Aldrich. All chemicals were used as received. Milli-Q® water was obtained from a Millipore Milli-Q equipment.

Synthesis. Typically, precipitations were driven by aging for 48 h at 25 ºC 100 mL of filtered solutions containing NaCl (100 mM), a chloride salt of Co(II), Ni(II), or a combination of the aforementioned divalent cations (keeping a total cationic concentration of 10 mM) in the presence of glycidol (400 mM). The solids were obtained by filtration, washed three time with water and then with ethanol, dried at room temperature.

Characterization of Solid Phases. All synthesized solids were characterized by powder X-ray diffraction (PXRD) using a graphite-filtered Cu K_α radiation (λ = 1.5406 Å), field emission on scanning electron microscopy (Carl Zeiss SUPRA 40), equipped with energy dispersive X-ray spectroscopy (EDS) probe. UV-Vis absorption spectra of the solid samples were recorded in a reflectance mode using an Ocean Optics spectrometer.

X-ray Absorption Spectroscopy. X-ray absorption spectroscopy (XAS) measurements were performed using the in-house X-ray absorption spectrometer from the Rigaku Company for Co and Ni K-edges. Co and Ni K-edges XANES+EXAFS spectra were measured at room temperature in transmission mode, in order to obtain representative information of the whole sample avoiding surface enrichment. Absorbents were prepared from fresh powder samples in pellets of 1.4 mm diameter and sealed with Kapton® tape (50 μm in thickness) to prevent the oxidation of the sample. The optimum amount of material for the measurements was calculated by the program XAFSMAS.[79] A Si(400) single crystal was used to obtain a monochromatic incident beam from a Mo anode target, using a current of 50 mA in the filament and a high voltage of 15 kV in the tube. Intensities of incident and transmitted X-rays were measured using an argon-filled proportional counter and a scintillation counter, respectively. EXAFS spectra were collected from 7550-8250 eV for Co K-edge, and between 8200-9200 eV for Ni K- edge. The incident photon energy was calibrated using the first inflection point of the Co K-edge (7709 eV) and the Ni K-edge (8333 eV) from reference foils of metallic Co and Ni, respectively. Ten spectra were taken with exposure times of 2 h each one. XANES data treatment was performed by subtracting the pre-edge background followed by normalization by extrapolation of a quadratic polynomial fitted at the post-edge region of the spectrum using ATHENA AUTOBK background removal

algorithm.[80] The quantitative analysis of the EXAFS results, were performed by modeling and fitting the insolated EXAFS oscillations. The EXAFS oscillations (k) were extracted from the experimental data with standard procedures using the Athena program. The k^3 weighted (k) data, to enhance the oscillations at higher k, were Fourier transformed. The Fourier transformation was calculated using the Hanning filtering function. EXAFS modeling was carried out using the ARTEMIS program which is part of the IFFEFIT package.[81]

The oxidation average state of Co ions was deduced from the position of the absorption edge at the K-Co based on a calibration curve. This curve was established with three reference samples as follows: metallic Co foil for Co(0), $Co_2Al(OH)_6(CO_3)_{0.5}.H_2O$ for Co(II) and $Co(NH_3)_6Cl_3$ for Co(III).

DFT+U Calculations. All calculations were performed in periodic boundary conditions employing density functional theory (DFT) as implemented in the Quantum Espresso code,[82] which is based on the pseudopotential approximation to represent the ion-electron interactions, and plane waves basis sets to expand the Kohn-Sham orbitals. Ultrasoft-type pseudopotentials were adopted, in combination with the PBE formalism to compute the exchange-correlation term.[83] The magnetic states are described through the Kohn-Sham Hamiltonian in the framework of spin polarized calculations, plus a Hubbard term. On the basis of our previous reports the incidence of the Hubbard parameter in the DFT+U calculations on the magnetic coupling and other properties was fixed to 4.5 eV for Co atoms. In the case of Ni atoms we explored the Hubbard parameter by screening its value between 3 and 8 eV. In all cases spin-orbit contributions were considered.[84] In concordance with previous reports on structurally related phases,[85, 86] we choose a Hubbard parameter value equal to 6 eV for Ni atoms. An energy threshold of 10^{-8} au was used for self-consistency, while for geometry optimization the convergence criteria were 10^{-6} au for the energy and of 10^{-3} au for the forces per atom. To improve the numerical convergence a first-order Methfessel-Paxton spreading was implemented. The simulations were carried out on supercell with specific ordering of the metal polyhedra within the layer and a general formula $(Co,Ni)^{Oh}{}_n(Co,Ni)^{Td}{}_2(OH)_{2n}Cl_2$, according to the representative metal composition obtained by epoxide route synthesis.[46] In this formula the nickel composition, X_{Ni} was varied for analyzed the effects of Ni content on the electronic structure. Brillouin zone sampling was performed on these supercells with a Monkhorst-Pack grid, checking for convergence with respect to the number of k-points. The size of supercells was $a = b = 9.35$ Å and $c = 14.7$ Å (isolated layer) for n = 8, and $a = b = 12.48$ Å and $c = 14.7$ Å (isolated layer) for n = 15. A 4x4x1 k-point grid was used in both cases.

10.1002/chem.202001944

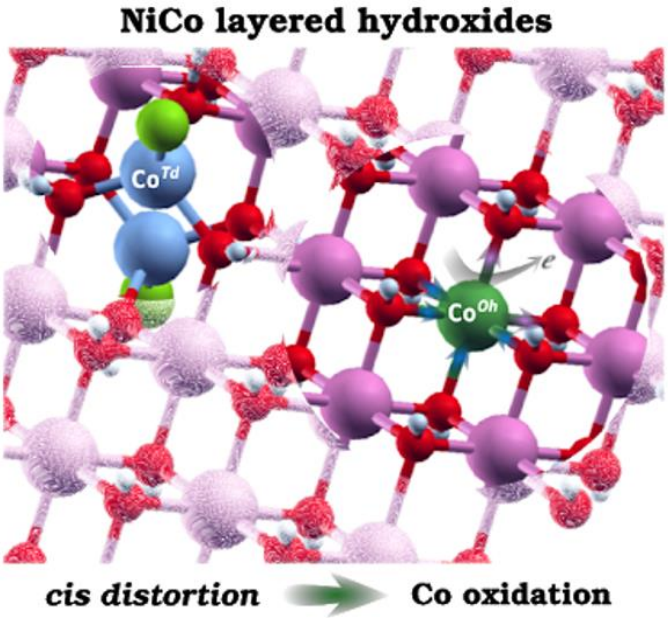

References

1. Shao, Y.; El-Kady, M. F.; Sun, J.; Li, Y.; Zhang, Q.; Zhu, M.; Wang, H.; Dunn, B.; Kaner, R. B., Design and Mechanisms of Asymmetric Supercapacitors. *Chemical Reviews* 2018, *118* (18), 9233-9280.

2. Nguyen, T.; Montemor, M. d. F., Metal Oxide and Hydroxide–Based Aqueous Supercapacitors: From Charge Storage Mechanisms and Functional Electrode Engineering to Need-Tailored Devices. *Advanced Science* 2019, *6* (9), 1801797.

3. Wang, Y.; Yan, D.; El Hankari, S.; Zou, Y.; Wang, S., Recent Progress on Layered Double Hydroxides and Their Derivatives for Electrocatalytic Water Splitting. *Advanced Science* 2018, *5* (8).

4. Wang, J.; Cui, W.; Liu, Q.; Xing, Z.; Asiri, A. M.; Sun, X., Recent Progress in Cobalt-Based Heterogeneous Catalysts for Electrochemical Water Splitting. *Advanced Materials* 2016, *28* (2), 215-230.

5. Wang, W.; Lu, Y.; Zhao, M.; Luo, R.; Yang, Y.; Peng, T.; Yan, H.; Liu, X.; Luo, Y., Controllable Tuning of Cobalt Nickel-Layered Double Hydroxide Arrays as Multifunctional Electrodes for Flexible Supercapattery Device and Oxygen Evolution Reaction. *ACS Nano* 2019, *13* (10), 12206-12218.

6. Zhang, X.; Hou, L.; Ciesielski, A.; Samorì, P., 2D Materials Beyond Graphene for High-Performance Energy Storage Applications. *Advanced Energy Materials* 2016, *6* (23), 1600671.

7. Tan, C.; Cao, X.; Wu, X.-J.; He, Q.; Yang, J.; Zhang, X.; Chen, J.; Zhao, W.; Han, S.; Nam, G.-H.; Sindoro, M.; Zhang, H., Recent Advances in Ultrathin Two-Dimensional Nanomaterials. *Chemical Reviews* 2017, *117* (9), 6225-6331.

8. Li, X.; Du, D.; Zhang, Y.; Xing, W.; Xue, Q.; Yan, Z., Layered double hydroxides toward high-performance supercapacitors. *Journal of Materials Chemistry A* 2017, *5* (30), 15460-15485.

9. Roger, I.; Shipman, M. A.; Symes, M. D., Earth-abundant catalysts for electrochemical and photoelectrochemical water splitting. *Nature Reviews Chemistry* 2017, *1* (1), 0003.

10. Deng, W.; Ji, X.; Chen, Q.; Banks, C. E., Electrochemical capacitors utilising transition metal oxides: An update of recent developments. *RSC Advances* 2011, *1* (7), 1171-1178.

11. Long, X.; Wang, Z.; Xiao, S.; An, Y.; Yang, S., Transition metal based layered double hydroxides tailored for energy conversion and storage. *Materials Today* 2016, *19* (4), 213-226.

12. Rui, X.; Tan, H.; Yan, Q., Nanostructured metal sulfides for energy storage. *Nanoscale* 2014, *6* (17), 9889-9924.

13. Wang, F.; Xiao, S.; Hou, Y.; Hu, C.; Liu, L.; Wu, Y., Electrode materials for aqueous asymmetric supercapacitors. *RSC Advances* 2013, *3* (32), 13059-13084.

14. Ma, X.; Wei, P.; Yang, Y.; Kang, H.; Guo, D.; Liu, L., One-pot synthesis of Ni-Co layered double hydroxide nanosheets as efficient catalysts for oxygen evolution reaction. *Materials Today Communications* 2019, *20*, 100596.

15. a) Gupta, V.; Gupta, S.; Miura, N., Statically deposited nanostructured Co_xNi_{1-x} layered double hydroxides as electrode materials for redox-supercapacitors. *Journal of Power Sources* 2008, *175* (1), 680-685. b) Liu, L.; Ma, K.-Y.; Liu, F.; Zhang, X.-B.; Cheng, J. P., Effects of Co/Ni Ratio on the Supercapacitive Properties of α-Form Hydroxides. European Journal of Inorganic Chemistry 2015, 2015 (14), 2448-2456.

16. Han, J.; Roh, K. C.; Jo, M. R.; Kang, Y. M., A novel co-precipitation method for one-pot fabrication of a Co-Ni multiphase composite electrode and its application in high energy-density pseudocapacitors. *Chemical Communications* 2013, *49* (63), 7067-7069.

17. Chen, H.; Hu, L.; Chen, M.; Yan, Y.; Wu, L., Nickel-cobalt layered double hydroxide nanosheets for high-performance supercapacitor electrode materials. *Advanced Functional Materials* 2014, *24* (7), 934-942.

18. Liang, B.; Chen, Y.; He, J.; Chen, C.; Liu, W.; He, Y.; Liu, X.; Zhang, N.; Roy, V. A. L., Controllable Fabrication and Tuned Electrochemical Performance of Potassium Co–Ni Phosphate Microplates as Electrodes in Supercapacitors. *ACS Appl. Mater. Interfaces* 2018, *10* (4), 3506-3514.

19. Patel, R.; Park, J. T.; Patel, M.; Dash, J. K.; Gowd, E. B.; Karpoormath, R.; Mishra, A.; Kwak, J.; Kim, J. H., Transition-metal-based layered double hydroxides tailored for energy conversion and storage. *Journal of Materials Chemistry A* 2018, *6* (1), 12-29.

20. Dong, T.; Zhang, X.; Li, M.; Wang, P.; Yang, P., Hierarchical flower-like Ni–Co layered double hydroxide nanostructures: synthesis and super performance. *Inorganic Chemistry Frontiers* 2018, *5* (12), 3033-3041.

21. Liu, X.; Ma, R.; Bando, Y.; Sasaki, T., A General Strategy to Layered Transition-Metal Hydroxide Nanocones: Tuning the Composition for High Electrochemical Performance. *Advanced Materials* 2012, *24* (16), 2148-2153.

22. Chen, G.; Liaw, S. S.; Li, B.; Xu, Y.; Dunwell, M.; Deng, S.; Fan, H.; Luo, H., Microwave-assisted synthesis of hybrid $Co_xNi_{1-x}(OH)_2$ nanosheets: Tuning the composition for high performance supercapacitor. *Journal of Power Sources* 2014, *251*, 338-343.

23. Wang, L.; Dong, Z. H.; Wang, Z. G.; Zhang, F. X.; Jin, J., Layered α-$Co(OH)_2$ Nanocones as Electrode Materials for Pseudocapacitors: Understanding the Effect of Interlayer Space on Electrochemical Activity. *Advanced Functional Materials* 2013, *23* (21), 2758-2764.

24. Liang, H.; Meng, F.; Cabán-Acevedo, M.; Li, L.; Forticaux, A.; Xiu, L.; Wang, Z.; Jin, S., Hydrothermal Continuous Flow Synthesis and Exfoliation of NiCo Layered Double Hydroxide Nanosheets for Enhanced Oxygen Evolution Catalysis. *Nano Lett.* 2015, *15* (2), 1421-1427.

25. Chen, H.; Cai, F.; Kang, Y.; Zeng, S.; Chen, M.; Li, Q., Facile assembly of Ni-Co hydroxide nanoflakes on carbon nanotube network with highly electrochemical capacitive. *ACS Applied Materials and Interfaces* 2014, *6* (22), 19630-19637.

26. Zhao, J.; Chen, J.; Xu, S.; Shao, M.; Zhang, Q.; Wei, F.; Ma, J.; Wei, M.; Evans, D. G.; Duan, X., Hierarchical NiMn Layered Double Hydroxide/Carbon Nanotubes Architecture with Superb Energy Density for Flexible Supercapacitors. *Advanced Functional Materials* 2014, *24* (20), 2938-2946.

27. Guo, X.; Liang, G.; Gu, A., Construction of nickel-doped cobalt hydroxides hexagonal nanoplates for advanced oxygen evolution electrocatalysis. *Journal of Colloid and Interface Science* 2019, *553*, 713-719.

28. Yang, J.; Yu, C.; Hu, C.; Wang, M.; Li, S.; Huang, H.; Bustillo, K.; Han, X.; Zhao, C.; Guo, W.; Zeng, Z.; Zheng, H.; Qiu, J., Surface-Confined Fabrication of Ultrathin Nickel Cobalt-Layered Double Hydroxide Nanosheets for High-Performance Supercapacitors. *Advanced Functional Materials* 2018, *28* (44), 1803272.

29. Li, Z.; He, S.; Ji, C.; Mi, H.; Lei, C.; Li, Z.; Pang, H.; Fan, Z.; Yu, C.; Qiu, J., Hierarchical Bimetallic Hydroxides Built by Porous Nanowire-Lapped Bundles with Ultrahigh Areal Capacity for Stable Hybrid Solid-State Supercapacitors. *Advanced Materials Interfaces* 2019, *6* (24), 1900959.

30. Li, P.; Duan, X.; Kuang, Y.; Li, Y.; Zhang, G.; Liu, W.; Sun, X., Tuning Electronic Structure of NiFe Layered Double Hydroxides with Vanadium Doping toward High Efficient Electrocatalytic Water Oxidation. *Advanced Energy Materials* 2018, *8* (15), 1703341.

31. Jain, A.; Shin, Y.; Persson, K. A., Computational predictions of energy materials using density functional theory. *Nature Reviews Materials* 2016, *1* (1), 15004.

32. Liang, W.; Chen, J.; Liu, Y.; Chen, S., Density-Functional-Theory Calculation Analysis of Active Sites for Four-Electron Reduction of O_2 on Fe/N-Doped Graphene. *ACS Catalysis* 2014, *4* (11), 4170-4177.

33. Seh, Z. W.; Kibsgaard, J.; Dickens, C. F.; Chorkendorff, I.; Nørskov, J. K.; Jaramillo, T. F., Combining theory and experiment in electrocatalysis: Insights into materials design. *Science* 2017, *355* (6321), eaad4998.

34. Himmetoglu, B.; Floris, A.; de Gironcoli, S.; Cococcioni, M., Hubbard-corrected DFT energy functionals: The LDA+U description of correlated systems. *International Journal of Quantum Chemistry* 2014, *114* (1), 14-49.

35. Hunt, D.; Garbarino, G.; Rodríguez-Velamazán, J. A.; Ferrari, V.; Jobbagy, M.; Scherlis, D. A., The magnetic structure of β-cobalt hydroxide and the effect of spin-orientation. *Phys. Chem. Chem. Phys.* 2016, *18*, 30407-30414.

36. Hunt, D.; Jobbagy, M.; Scherlis, D. A., Interplay of Coordination Environment and Magnetic Behavior of Layered Co(II) Hydroxichlorides: A DFT+U Study. *Inorganic Chemistry* 2018, *57* (9), 4989-4996.

37. Lu, Z.; Qian, L.; Tian, Y.; Li, Y.; Sun, X.; Duan, X., Ternary NiFeMn layered double hydroxides as highly-efficient oxygen evolution catalysts. *Chemical Communications* 2016, *52* (5), 908-911.

38. Ding, S.; Du, X.; Yang, Y.; Wang, P.; Zhang, Z.; Hao, X.; Peng, C.; Guan, G., Theoretical and experimental investigations of the electronic/ionic conductivity and deprotonation of $Ni_{3-x}Co_xAl$-LDHs in an electrochemical energy storage system. *Physical Chemistry Chemical Physics* 2018, *20* (25), 17313-17323.

39. Friebel, D.; Louie, M. W.; Bajdich, M.; Sanwald, K. E.; Cai, Y.; Wise, A. M.; Cheng, M.-J.; Sokaras, D.; Weng, T.-C.; Alonso-Mori, R.; Davis, R. C.; Bargar, J. R.; Nørskov, J. K.; Nilsson, A.; Bell, A. T., Identification of Highly Active Fe Sites in (Ni,Fe)OOH for Electrocatalytic Water Splitting. *Journal of the American Chemical Society* 2015, *137* (3), 1305-1313.

40. Kwon, N. H.; Kim, M.; Jin, X.; Lim, J.; Kim, I. Y.; Lee, N.-S.; Kim, H.; Hwang, S.-J., A rational method to kinetically control the rate-determining step to explore efficient electrocatalysts for the oxygen evolution reaction. *NPG Asia Materials* 2018, *10* (7), 659-669.

41. Bi, Y.; Cai, Z.; Zhou, D.; Tian, Y.; Zhang, Q.; Zhang, Q.; Kuang, Y.; Li, Y.; Sun, X.; Duan, X., Understanding the incorporating effect of Co^{2+}/Co^{3+} in NiFe-layered double hydroxide for electrocatalytic oxygen evolution reaction. *Journal of Catalysis* 2018, *358*, 100-107.

42. Musella, E.; Gualandi, I.; Scavetta, E.; Rivalta, A.; Venuti, E.; Christian, M.; Morandi, V.; Mullaliu, A.; Giorgetti, M.; Tonelli, D., Newly developed electrochemical synthesis of Co-based layered double hydroxides: toward noble metal-free electro-catalysis. *Journal of Materials Chemistry A* 2019, *7* (18), 11241-11249.

43. Akama, S.; Kobayashi, W.; Amaha, K.; Niwa, H.; Nitani, H.; Moritomo, Y., Local structures around the substituted elements in mixed layered oxides. *Scientific Reports* 2017, *7* (1), 43791.

44. Dumas, A.; Mizrahi, M.; Martin, F.; Requejo, F. G., Local and Extended-Order Evolution of Synthetic Talc during Hydrothermal Synthesis: Extended X-ray Absorption Fine Structure, X-ray Diffraction, and Fourier Transform Infrared Spectroscopy Studies. *Cryst. Growth Des.* 2015, *15* (11), 5451-5463.

45. Arencibia, N.; Oestreicher, V.; Viva, F. A.; Jobbágy, M., Nanotextured alpha Ni(II)-Co(II) hydroxides as supercapacitive active phases. *RSC Advances* 2017, *7* (10), 5595-5600.

46. Oestreicher, V.; Jobbágy, M., One pot synthesis of $Mg_2Al(OH)_6Cl{\cdot}1.5H_2O$ layered double hydroxides: The epoxide route. *Langmuir* 2013, *29* (39), 12104-12109.

47. Oestreicher, V.; Fábregas, I.; Jobbágy, M., One-pot epoxide-driven synthesis of $M_2Al(OH)_6Cl{\cdot}1.5H_2O$ layered double hydroxides: Precipitation mechanism and relative stabilities. *Journal of Physical Chemistry C* 2014, *118* (51), 30274-30281.

48. Oestreicher, V.; Jobbágy, M., On Demand One-Pot Mild Preparation of Layered Double Hydroxides and Their Hybrid Forms: Advances through the Epoxide Route. *Chemistry – A European Journal* 2019, *25* (54), 12611-12619.

49. Liu, Z.; Ma, R.; Osada, M.; Takada, K.; Sasaki, T., Selective and controlled synthesis of α- and β-cobalt hydroxides in highly developed hexagonal platelets. *Journal of the American Chemical Society* 2005, *127* (40), 13869-13874.

50. Oestreicher, V.; Hunt, D.; Torres-Cavanillas, R.; Abellán, G.; Scherlis, D. A.; Jobbágy, M., Halide-Mediated Modification of Magnetism and Electronic Structure of α-Co(II) Hydroxides: Synthesis, Characterization, and DFT+U Simulations. *Inorganic Chemistry* 2019, *58* (14), 9414-9424.

51. Ma, R. Z.; Liu, Z. P.; Takada, K.; Fukuda, K.; Ebina, Y.; Bando, Y.; Sasaki, T., Tetrahedral Co(II) coordination in alpha-type cobalt hydroxide: Rietveld refinement and X-ray absorption spectroscopy. *Inorganic Chemistry* 2006, *45* (10), 3964-3969.

52. Kurmoo, M., Magnetic metal-organic frameworks. *Chemical Society Reviews* 2009, *38* (5), 1353-1379.

53. Hawthorne, F. C.; Sokolova, E., Simonkolleite, $Zn_5(OH)_8Cl_2(H_2O)$, a decorated interrupted-sheet structure of the form $[Mf_2]_4$. *Canadian Mineralogist* 2002, *40*, 939-946.

54. Neilson, J. R.; Schwenzer, B.; Seshadri, R.; Morse, D. E., Kinetic control of intralayer cobalt coordination in layered hydroxides: $Co_{1-05x}{}^{oct}Co_x{}^{tet}(OH)_2(CI)_x(H_2O)_n$. *Inorganic Chemistry* 2009, *48* (23), 11017-11023.

55. Neilson, J. R.; Kurzman, J. A.; Seshadri, R.; Morse, D. E., Cobalt coordination and clustering in α-$Co(OH)_2$ revealed by synchrotron X-ray total scattering. *Chemistry - A European Journal* 2010, *16* (33), 9998-10006.

56. Neilson, J. R.; Morse, D. E.; Melot, B. C.; Shoemaker, D. P.; Kurzman, J. A.; Seshadri, R., Understanding complex magnetic order in disordered cobalt hydroxides through analysis of the local structure. *Physical Review B - Condensed Matter and Materials Physics* 2011, *83* (9).

57. Sławiński, W. A.; Sjåstad, A. O.; Fjellvåg, H., Stacking Faults and Polytypes for Layered Double Hydroxides: What Can We Learn from Simulated and Experimental X-ray Powder Diffraction Data? *Inorganic Chemistry* 2016, *55* (24), 12881-12889.

58. Kamath, P. V.; Dixit, M.; Indira, L.; Shukla, A. K.; Kumar, V. G.; Munichandraiah, N., Stabilized α-$Ni(OH)_2$ as Electrode Material for Alkaline Secondary Cells. *Journal of the Electrochemical Society* 1994, *141* (11), 2956-2959.

59. Kamath, P. V.; Annal Therese, G. H.; Gopalakrishnan, J., On the Existence of Hydrotalcite-Like Phases in the Absence of Trivalent Cations. *Journal of Solid State Chemistry* 1997, *128* (1), 38-41.

60. Soler-Illia, G. J. A. A.; Jobbagy, M.; Regazzoni, A. E.; Blesa, M. A., Synthesis of nickel hydroxide by homogeneous alkalinization. Precipitation mechanism. *Chemistry of Materials* 1999, *11* (11), 3140-3146.

61. McClure, D. S., Optical Spectra of Transition-Metal Ions in Corundum. *The Journal of Chemical Physics* 1962, *36* (10), 2757-2779.

62. Rives, V.; Kannan, S., Layered double hydroxides with the hydrotalcite-type structure containing Cu^{2+}, Ni^{2+} and Al^{3+}. *Journal of Materials Chemistry* 2000, *10* (2), 489-495.

63. Mansour, A. N.; Melendres, C. A., Analysis of X-ray Absorption Spectra of Some Nickel Oxycompounds Using Theoretical Standards. *The Journal of Physical Chemistry A* 1998, *102* (1), 65-81.

64. Ma, R.; Takada, K.; Fukuda, K.; Iyi, N.; Bando, Y.; Sasaki, T., Topochemical synthesis of monometallic (Co^{2+}-Co^{3+}) layered double hydroxide and its exfoliation into positively charged $Co(OH)_2$ nanosheets. *Angewandte Chemie - International Edition* 2008, *47* (1), 86-89.

65. Shannon, R. D., Revised Effective Ionic-Radii and Systematic Studies of Interatomic Distances in Halides and Chalcogenides. *Acta Crystallographica Section A* 1976, *32* (SEP1), 751-767.

66. Choy, J. H.; Kwon, Y. M.; Han, K. S.; Song, S. W.; Chang, S. H., Intra- and inter-layer structures of layered hydroxy double salts, $Ni_{1-x}Zn_{2x}(OH)_2(CH_3CO_2)_{2x}\cdot nH_2O$. *Materials Letters* 1998, *34* (3-6), 356-363.

67. Tessier, C.; Guerlou-Demourgues, L.; Faure, C.; Demourgues, A.; Delmas, C., Structural study of zinc-substituted nickel hydroxides. *Journal of Materials Chemistry* 2000, *10* (5), 1185-1193.

68. Pandya, K. I.; O'Grady, W. E.; Corrigan, D. A.; McBreen, J.; Hoffman, R. W., Extended X-ray absorption fine structure investigations of nickel hydroxides. *Journal of Physical Chemistry* 1990, *94* (1), 21-26.

69. Leroux, F.; Moujahid, E.; Taviot-Gueho, C.; Besse, J. P., Effect of layer charge modification for Co-Al layered double hydroxides: study by X-ray absorption spectroscopy. *Solid State Sciences* 2001, *3* (1-2), 81-92.

70. Bar, A. K.; Pichon, C.; Sutter, J.-P., Magnetic anisotropy in two- to eight-coordinated transition–metal complexes: Recent developments in molecular magnetism. *Coordination Chemistry Reviews* 2016, *308*, 346-380.

71. Cremades, E.; Echeverría, J.; Alvarez, S., The Trigonal Prism in Coordination Chemistry. *Chemistry – A European Journal* 2010, *16* (34), 10380-10396.

72. Halcrow, M. A., Jahn–Teller distortions in transition metal compounds, and their importance in functional molecular and inorganic materials. *Chemical Society Reviews* 2013, *42* (4), 1784-1795.

73. Echeverría, J.; Cremades, E.; Amoroso, A. J.; Alvarez, S., Jahn–Teller distortions of six-coordinate Cu^{II} compounds: *cis* or *trans*? *Chemical Communications* 2009, (28), 4242-4244.

74. Jansze, S. M.; Severin, K., Clathrochelate Metalloligands in Supramolecular Chemistry and Materials Science. *Accounts of Chemical Research* 2018, *51* (9), 2139-2147.

75. Pantani, O.; Naskar, S.; Guillot, R.; Millet, P.; Anxolabéhère-Mallart, E.; Aukauloo, A., Cobalt Clathrochelate Complexes as Hydrogen-Producing Catalysts. *Angewandte Chemie International Edition* 2008, *47* (51), 9948-9950.

76. Voloshin, Y. Z.; Varzatskii, O. A.; Vorontsov, I. I.; Antipin, M. Y., Tuning a Metal's Oxidation State: The Potential of Clathrochelate Systems. *Angewandte Chemie* 2005, *117* (22), 3466-3468.

77. Tomyn, S.; Shylin, S. I.; Bykov, D.; Ksenofontov, V.; Gumienna-Kontecka, E.; Bon, V.; Fritsky, I. O., Indefinitely stable iron(IV) cage complexes formed in water by air oxidation. *Nature Communications* 2017, *8* (1), 14099.

78. Dinh Nguyen, M. T.; Charlot, M.-F.; Aukauloo, A., Structural, Electronic, and Theoretical Description of a Series of Cobalt Clathrochelate Complexes in the Co(III), Co(II) and Co(I) Oxidation States. *The Journal of Physical Chemistry A* 2011, *115* (5), 911-922.

79. Klementiev, K. V., *XAFSmass, freeware, www.cells.es/Beamlines/CLAESS/software/xafsmass.html*.

80. Ravel, B.; Newville, M., ATHENA, ARTEMIS, HEPHAESTUS: data analysis for X-ray absorption spectroscopy using IFEFFIT. *Journal of Synchrotron Radiation* 2005, *12* (4), 537-541.

81. Newville, M., IFEFFIT : interactive XAFS analysis and FEFF fitting. *Journal of Synchrotron Radiation* 2001, *8* (2), 322-324.

82. Giannozzi, P.; Baroni, S.; Bonini, N.; Calandra, M.; Car, R.; Cavazzoni, C.; Ceresoli, D.; Chiarotti, G. L.; Cococcioni, M.; Dabo, I.; Dal Corso, A.; de Gironcoli, S.; Fabris, S.; Fratesi, G.; Gebauer, R.; Gerstmann, U.; Gougoussis, C.; Kokalj, A.; Lazzeri, M.; Martin-Samos, L.; Marzari, N.; Mauri, F.; Mazzarello, R.; Paolini, S.; Pasquarello, A.; Paulatto, L.; Sbraccia, C.; Scandolo, S.; Sclauzero, G.; Seitsonen, A. P.; Smogunov, A.; Umari, P.; Wentzcovitch, R. M., QUANTUM ESPRESSO: a modular and open-source software project for quantum simulations of materials. *Journal of Physics: Condensed Matter* 2009, *21* (39), 395502.

83. Perdew, J. P.; Burke, K.; Ernzerhof, M., Generalized Gradient Approximation Made Simple. *Phys. Rev. Lett.* 1996, *77* (18), 3865-3868.

84. Dal Corso, A.; Conte, A. M., Spin-orbit coupling with ultrasoft pseudopotentials: Application to Au and Pt. *Physical Review B - Condensed Matter and Materials Physics* 2005, *71* (11).

85. Nagli, M.; Caspary Toroker, M., Communication: Nickel hydroxide as an exceptional deviation from the quantum size effect. *The Journal of Chemical Physics* 2018, *149* (14), 141103.

86. Nagli, M.; Caspary Toroker, M., The electronic structure of two-dimensional transition metal hydroxide monolayers and heterostructures. *Solid State Ionics* 2018, *314*, 149-155.

87. He, Y.; Liu, X.; Chen, G.; Pan, J.; Yan, A.; Li, A.; Lu, X.; Tang, D.; Zhang, N.; Qiu, T.; Ma, R.; Sasaki, T., Synthesis of Co(II)-Fe(III) Hydroxide Nanocones with Mixed Octahedral/Tetrahedral Coordination toward Efficient Electrocatalysis. Chemistry of Materials 2020, 32 (10), 4232-4240.